Magnetoexciton transitions in GaAs-$Ga_{1-x}Al_xAs$ quantum wells

2002 J. Phys.: Condens. Matter 14 1021

(http://iopscience.iop.org/0953-8984/14/5/307)

INSTITUTE OF PHYSICS PUBLISHING JOURNAL OF PHYSICS: CONDENSED MATTER

J. Phys.: Condens. Matter **14** (2002) 1021–1033 PII: S0953-8984(02)28582-3

Magnetoexciton transitions in GaAs–$Ga_{1-x}Al_xAs$ quantum wells

Z Barticevic[1], M Pacheco[2], C A Duque[3] and L E Oliveira[4]

[1] Depto. de Física, Universidad Técnica Federico Santa María, Casilla 110-V, Valparaíso, Chile
[2] Depto. de Física, Universidad de Santiago de Chile, Casilla 307, Santiago, Chile
[3] Depto. de Física, Universidad de Antioquia, AA 1226, Medellín, Colombia
[4] Inst. de Física, Univ. Estadual de Campinas-Unicamp, CP 6165, Campinas-SP, Brazil

Received 6 September 2001
Published 25 January 2002
Online at stacks.iop.org/JPhysCM/14/1021

Abstract

A theoretical study of the internal transitions of confined magnetoexcitons in GaAs–$Ga_{1-x}Al_xAs$ quantum wells is presented, with the magnetic field applied along the growth direction of the semiconductor heterostructure. The various exciton-envelope wavefunctions are described as products of electron and hole solutions of the associated quantum-well potentials and symmetry-adapted Gaussian functions. The magnetoexciton states are simultaneously obtained by diagonalizing the appropriate Hamiltonian in the effective-mass approximation. Exciton internal transitions are theoretically investigated by studying the allowed magnetoexcitonic transitions using far-infrared (terahertz) radiation circularly polarized in the plane of the quantum well. Theoretical results are obtained for both the intramagnetoexciton transition energies and oscillator strengths associated with excitations from 1s-like to 2s-, $2p_{\pm}$-, and $3p_{\pm}$-like magnetoexciton states, and from $2p_{-}$- to 2s-like exciton states. The present results are compared with previous theoretical work and available optically detected resonance measurements.

1. Introduction

The understanding of the physics underlying electronic, impurity and exciton states in man-made low-dimensional systems, such as semiconductor heterostructures, is of paramount importance as nowadays a wide range of semiconductor devices are based on artificial semiconductor systems. The study of the optical properties of semiconductor heterostructures provides worthy information on the physical nature of confined electrons, holes, and Coulomb-bound states such as impurities and excitons. Effects arising from quantum confinement (due to the reduced dimensionality) of low-dimensional semiconductor heterostructures may be of considerable relevance for potential applications in novel electronic and optoelectronic semiconductor devices. Advances in nanofabrication techniques which have occurred in these past two decades have made it possible to realize semiconductor nanostructures with controlled

thicknesses and sharp interfaces. For a number of reasons, most experimental and theoretical work in low-dimensional semiconductor heterostructures have been concentrated in III–V semiconductor systems, and type I GaAs–$Ga_{1-x}Al_xAs$ quantum wells (QWs), symmetric and double coupled QWs, multiple quantum wells (MQWs), quantum-well wires (QWWs), quantum dots (QDs), superlattices (SLs), and so on, have been widely studied [1, 2]. Also, it is well known that excitons essentially dominate the optical properties of semiconductor heterostructures. In that respect, the additional quantum confinement of electrons and holes in GaAs–$Ga_{1-x}Al_xAs$ MQWs and SLs leads to the formation of carrier subbands with dispersions depending on the interwell coupling. Therefore, exciton states, which are correlated electron–hole (e–h) pairs held together by the Coulomb attraction, may be significantly modified with respect to those of the host GaAs and $Ga_{1-x}Al_xAs$ semiconductor materials, and numerous theoretical and experimental studies have been motivated by the pronounced effects of quasi-two-dimensionality in the excitonic features of the optical spectra. In particular, an external perturbation such as an applied magnetic field perpendicular to the GaAs and $Ga_{1-x}Al_xAs$ semiconductor layers is a powerful tool which is expected to provide valuable information on carrier subbands and exciton states via magneto-optical studies.

Of particular interest to this work, excitons in GaAs–$Ga_{1-x}Al_xAs$ QWs and MQWs are correlated e–h pairs which behave as hydrogenic-like systems, with effective Bohr radii and binding energies of the order of 100 Å and 5–10 meV, respectively. Confined excitons in GaAs–$Ga_{1-x}Al_xAs$ QWs and MQWs under magnetic fields applied in the growth direction reveal themselves as a series of hydrogenic-like ground and excited magnetoexciton states. In type II GaAs/AlAs QWs, Hodge *et al* [3] have used a photoinduced absorption technique and were able to observe internal excitonic transitions. In type I GaAs–$Ga_{1-x}Al_xAs$ MQWs, the internal transition energies among the various exciton states all lie in the far-infrared region (FIR—of the order of 10 meV or 2.4 THz), and one may therefore probe the terahertz internal dynamics of magnetoexcitons by using either FIR laser light [4–7] or a free electron laser as the FIR source [8–11]. By using a recently developed optically detected resonance (ODR) technique, which combines the sensitivity of visible/near IR photon detection with FIR excitation and allows one to monitor changes in photoluminescence (PL) that result from FIR absorption, Salib *et al* [4] and Cerne *et al* [8] have been able to observe internal magnetoexciton transitions in GaAs–$Ga_{1-x}Al_xAs$ MQWs. In particular, the study by Salib *et al* [4] revealed several internal excitonic transitions and found the $1s \rightarrow 2p_+$ heavy-hole (hh) exciton transition [12][5] as dominant in GaAs–$Ga_{0.7}Al_{0.3}As$ MQWs of $L_w = 80$ Å and $L_w = 125$ Å well width. Salib *et al* [4] also found the strength of the intraexcitonic features much *weaker* in $L_w = 200$ Å well-width samples, a behavior which contrasts with their calculation of the oscillator strength for the $1s \rightarrow 2p$ transition which indicates a substantial *increase* going from a strictly two-dimensional (2D) to a strictly three-dimensional (3D) hydrogenic system. One should also point out that Salib *et al* [4] assign a 'weak' feature and a 'very weak' feature in the ODR spectra to hh magnetoexciton $1s \rightarrow 3p_+$ and $1s \rightarrow 4p_+$ transitions, respectively, based primarily on the magnitude of the energy separations with respect to the $1s \rightarrow 2p_+$ transition. Also, some features present in the ODR spectra by Salib *et al* [4] were attributed to hole cyclotron resonances (CRs) and others termed as 'of uncertain origin'. In a simultaneous and independent study, Cerne *et al* [8] monitored changes in the excitonic PL that are induced by FIR radiation with the electric field polarized in the plane of the QW, and observed resonant FIR absorption by confined magnetoexcitons in a

[5] Exciton states in QWs under growth-direction applied magnetic fields cannot unambiguously be classified as hydrogenic 1s, $2p_+$, etc, or as light- or heavy-hole states, although one finds this practice very often in the literature. Here we follow the notation used in the experimental work (see [4–10]), and refer to the study below (see [13]) for a detailed discussion on the symmetry of exciton states in QWs under magnetic fields.

number of GaAs–$Ga_{1-x}Al_xAs$ QWs under magnetic fields applied perpendicular to the well interfaces. The dominant resonance was assigned to the $1s \rightarrow 2p_+$ hh exciton transition, and was found [8] to persist even when the FIR electric field was comparable to the electric field which binds the exciton. Cerne *et al* [8] have also presented results for the 1s–2s hh exciton separation (obtained from PL and PLE measurements), and for ODR features which they assign to electron CR, although they point out that its dispersion agree almost as well with the predicted [13, 14] $2p_- \rightarrow 2s$ excitonic transition. More recently, Nickel *et al* [5–7] have used ODR spectroscopy to study electron and hole CRs and various internal excitonic transitions in a GaAs–$Al_{0.3}Ga_{0.7}As$ MQW structure with 30 repetitions of a $L_w = 125$ Å wide well and a $L_b = 125$ Å wide barrier. The two principal hole CR transitions were identified by comparison with theoretical calculations as originating from different spin states of the highest hh subband (hh1) Landau level ($|0, +3/2\rangle \rightarrow |1, +3/2\rangle$ and $|0, -3/2\rangle \rightarrow |1, -3/2\rangle$) and, in addition to nearly-degenerate $1s \rightarrow 2p_+$ internal exciton transitions, Nickel *et al* [5–7] have observed two $1s \rightarrow 2p_-$ intraexcitonic transitions resulting from the two distinct hh magnetoexcitons, i.e. the [+1/2, +3/2] (an exciton formed by an $m_J = +1/2$ electron and an $m_J = +3/2$ hole) and [−1/2, −3/2] magnetoexcitons. Nickel *et al* [5–7] have also tentatively identified some highest energy excitonic features as the $1s \rightarrow 3p_+$ transition (assumed to be nearly degenerate as in the $2p_+$ case), and $1s \rightarrow 3p_-$ transitions, and concluded by stating that more work is necessary to confirm the $2p_\pm$ assignments, to resolve the nature of the higher energy intraexcitonic transitions, and to observe light-hole (lh) CR and associated intraexcitonic transitions. From the theoretical point of view, Duque *et al* [15] have performed a study of $1s \rightarrow 2p_\pm$, $1s \rightarrow 3p_\pm$, and $1s \rightarrow 4p_\pm$ lh and hh magnetoexcitonic transition energies in GaAs–$Ga_{1-x}Al_xAs$ QWs within a variational procedure in the effective-mass approximation, and although some of the theoretical magnetoexciton transition energies agree very well with experimental measurements, other calculated results only reproduce qualitative features of experiment. Duque *et al* [15] have also demonstrated that several theoretically possible magnetoexciton transitions do not show up in the experimental spectra and concluded that further theoretical study of the intraexcitonic absorption lineshape would certainly be of considerable importance for a better explanation of the experimental measurements.

In order to provide a better understanding of the terahertz internal dynamics of confined magnetoexcitons in GaAs–$Ga_{1-x}Al_xAs$ QWs and of the ODR experimental data by Salib *et al* [4], Nickel *et al* [5–7], and Cerne *et al* [8–10], here we perform a theoretical study in the effective-mass approximation of the various intraexcitonic transitions in GaAs–$Ga_{1-x}Al_xAs$ QWs under magnetic fields applied along the QW growth direction. We assume a parabolic dispersion for electrons and a four-band diagonal approximation for holes, with the various magnetoexciton states obtained by expanding the corresponding exciton-envelope wave functions in terms of appropriate Gaussian functions.

The paper is organized as follows. The theoretical framework for calculating the magnetoexciton envelope wavefunctions and various intraexcitonic transitions is detailed in section 2. Calculated results and discussion of comparison with available experimental measurements is given in section 3. Finally, summary and conclusions are found in section 4.

2. Theoretical framework

We work in the effective-mass approximation and are interested in Wannier-exciton states in GaAs–$Ga_{1-x}Al_xAs$ QWs of width L_w in the presence of a magnetic field parallel to the growth direction of the heterostructure. We ignore small departures from inversion symmetry which occur in GaAs zincblend semiconductors. In bulk GaAs, the conduction band is an s-type twofold spin-degenerate Γ_6 state at $k = 0$, whereas the valence band is p-type threefold

degenerate at $k = 0$, if one ignores spin. When spin is included, the spin–orbit interaction causes the valence-band edge to be split into a low-energy $J = 1/2$ (J is the total angular momentum) twofold-degenerate Γ_7 split off state and a valence-band edge $J = 3/2$ fourfold-degenerate Γ_8 state. We assume the spin–orbit splitting to be large enough that the interaction between $J = 3/2$ and $1/2$ states may be disregarded. Moreover, couplings between conduction and valence bands as well as couplings to more distant bands are ignored altogether, so that the valence band may be described by the Luttinger [16] Hamiltonian. We note that in bulk GaAs, away from Γ, the Γ_8 state splits into a twofold lh($J_z^{\rm lh} = \pm 1/2$) band and a twofold hh($J_z^{\rm hh} = \pm 3/2$) band, although, for a QW or SL, the hh and lh bands are separated even at Γ. In the effective-mass approximation, and having made the above considerations, one may then write the ith wavefunction of an exciton at rest in a GaAs–$Ga_{1-x}Al_xAs$ QW (we assume square-well potentials for the conduction and valence bands) as a linear combination of products of electron- and hole-Bloch functions associated to the conduction- and valence-band edges, respectively, i.e.

$$\Psi^i_{\rm ex}(\vec{r}_{\rm e}, \vec{r}_{\rm h}) = \sum_{J_z^{\rm e}, J_z^{\rm h}} F^i_{J_z^{\rm e}, J_z^{\rm h}}(\vec{r}_{\rm e}, \vec{r}_{\rm h}) \phi^c_{J_z^{\rm e}}(\vec{r}_{\rm e}) \hat{T} \phi^v_{J_z^{\rm h}}(\vec{r}_{\rm h}) \tag{2.1}$$

where $\vec{r}_{\rm e}, \vec{r}_{\rm h}$ denote the electron and hole coordinates, $\phi^c_M(\vec{r}_{\rm e})$, $\phi^v_{M'}(\vec{r}_{\rm h})$ correspond to the Bloch functions of the Γ_6 conduction- and Γ_8 valence-band edges, respectively, and $J_z^{\rm e} = (-1/2, +1/2)$ and $J_z^{\rm h} = (+3/2, +1/2, -1/2, -3/2)$ are the magnetic quantum numbers for the conduction electron and valence hole, respectively. $\hat{T}$ is the time inversion operator transforming the Bloch function of the valence-band edge electron into that of the corresponding hole. For simplicity, we may assume the relative motion of the carriers and that of the center of mass as independent, although one may only make this separation in the plane of the well [17, 18], and write $F^i_{J_z^{\rm e}, J_z^{\rm h}}(\vec{r}_{\rm e}, \vec{r}_{\rm h}) \equiv F^i_{J_z^{\rm e}, J_z^{\rm h}}(\vec{\rho}, z_{\rm e}, z_{\rm h})$, where $\vec{\rho}$ is the e–h relative coordinate in the plane of the QW. The $F^i_{J_z^{\rm e}, J_z^{\rm h}}(\vec{\rho}, z_{\rm e}, z_{\rm h})$ exciton-envelope wavefunctions are the solutions of the matrix equation

$$\sum_{J_z^{\prime e}, J_z^{\prime h}} (H^{\rm ex})_{J_z^{\rm e}, J_z^{\rm h}, J_z^{\prime e}, J_z^{\prime h}} F^i_{J_z^{\prime e}, J_z^{\prime h}}(\vec{\rho}, z_{\rm e}, z_{\rm h}) = E^i_{\rm ex} F^i_{J_z^{\rm e}, J_z^{\rm h}}(\vec{\rho}, z_{\rm e}, z_{\rm h}) \tag{2.2}$$

where $H^{\rm ex}$ is the effective-mass Hamiltonian operator which includes the effective-mass kinetic and magnetic energies of the conduction electron and valence hole in the presence of the growth-direction applied magnetic field, the screened e–h Coulomb interaction, and the electron and hole QW confining potentials. Equation (2.2) reduces to two four-dimensional equations for both $J_z^{\rm e} = \pm 1/2$ spin states of the conduction band, if one disregards the small contribution of the e–h exchange interaction.

In what follows, we will restrict our attention to independent excitons and discard the off-diagonal elements in the hole Hamiltonian, i.e. we neglect effects due to hole–subband mixing in the calculation. In addition, we ignore effects due to the small difference in the dielectric constant of well and barrier materials, i.e. image-charge effects are not considered and the e–h Coulomb interaction is assumed to be screened by an average static dielectric constant of the GaAs and $Ga_{1-x}Al_xAs$ bulk materials. The values of the potential-well barriers $V_c(z_{\rm e})$ and $V_v(z_{\rm h})$ are determined from the Al concentration and assumed to be 65 and 35% of the total energy-bandgap discontinuity, respectively. Although actual measurements are for GaAs–$Ga_{0.7}Al_{0.3}As$ SLs, for simplicity, we have also ignored SL tunneling effects and performed calculations for single isolated GaAs–$Ga_{0.7}Al_{0.3}As$ QWs.

We may now expand the exciton-envelope wavefunctions $F^i_{J_z^{\rm e}, J_z^{\rm h}}(\vec{\rho}, z_{\rm e}, z_{\rm h})$, which depend on the e–h relative coordinates $\vec{\rho} = (\rho, \phi)$ for motion parallel to the QW interfaces and on coordinates $z_{\rm e}$ and $z_{\rm h}$ for motion along the growth-direction z, in terms of single-particle

solutions $f_n^{J_z^e}(z_e)$ and $f_m^{J_z^h}(z_h)$ of the effective-mass equation for electron or hole motion, respectively, along the z-axis of the QW, i.e. $f_n^{J_z^e}(z_e)$ and $f_m^{J_z^h}(z_h)$ are solutions of

$$-\frac{\hbar^2}{2m_e^*}\frac{d^2 f_n^{J_z^e}(z_e)}{dz^2} + V_c(z_e) f_n^{J_z^e}(z_e) = \varepsilon_n^e f_n^{J_z^e}(z_e) \tag{2.3}$$

where $V_c(z_e)$ is the electron-barrier QW potential, and a corresponding equation for J_z^h holes. The exciton-envelope wavefunction $F^i_{J_z^e,J_z^h}(\vec{\rho}, z_e, z_h)$ may therefore be written as [19]

$$F^i_{J_z^e,J_z^h}(\vec{\rho}, z_e, z_h) = \sum_{n,m} \psi_{n,m}^{J_z^e,J_z^h,i}(\rho,\phi) f_n^{J_z^e}(z_e) f_m^{J_z^h}(z_h) \tag{2.4}$$

with

$$\psi_{n,m}^{J_z^e,J_z^h,i}(\rho,\phi) = \sum_j C_{n,m,j}^{J_z^e,J_z^h,i} \rho^{|s|} e^{is\phi} e^{-\frac{\rho^2}{\lambda_j^2}} \tag{2.5}$$

where the expansion is made in a restricted set of Gaussian functions with appropriate length parameters λ_j, and s is an integer associated with the conserved z component of the total angular momentum [19].

The hh and lh exciton Hamiltonians may be written as [16]

$$H^{exc}_{\pm 3/2} = -\frac{1}{m_e}\frac{\partial^2}{\partial z_e^2} + V_c(z_e) - \frac{1}{m_{h\perp}^{\pm 3/2}}\frac{\partial^2}{\partial z_h^2} + V_v(z_h) + \left(\frac{1}{m_e} + \frac{1}{m_{h\parallel}^{\pm 3/2}}\right)\left(-\nabla_{\vec{\rho}}^2 + \frac{\gamma^2\rho^2}{4}\right) + \left(\frac{1}{m_e} - \frac{1}{m_{h\parallel}^{\pm 3/2}}\right)\gamma L_z \pm \left(3\kappa + \frac{27}{4}q\right)\gamma - \frac{2}{\varepsilon|\boldsymbol{r}_e - \boldsymbol{r}_h|} \pm \frac{g_e}{2}\gamma \tag{2.6}$$

$$H^{exc}_{\pm 1/2} = -\frac{1}{m_e}\frac{\partial^2}{\partial z_e^2} + V_c(z_e) - \frac{1}{m_{h\perp}^{\pm 1/2}}\frac{\partial^2}{\partial z_h^2} + V_v(z_h) + \left(\frac{1}{m_e} + \frac{1}{m_{h\parallel}^{\pm 1/2}}\right)\left(-\nabla_{\vec{\rho}}^2 + \frac{\gamma^2\rho^2}{4}\right) + \left(\frac{1}{m_e} - \frac{1}{m_{h\parallel}^{\pm 1/2}}\right)\gamma L_z \pm \left(\kappa + \frac{1}{4}q\right)\gamma - \frac{2}{\varepsilon\,|\boldsymbol{r}_e - \boldsymbol{r}_h|} \pm \frac{g_e}{2}\gamma \tag{2.7}$$

respectively, with L_z as the operator for the orbital angular momentum in the z direction, and $\nabla_{\vec{\rho}}^2$ as the 2D Laplacian in the QW plane. Energies are expressed in units of Rydbergs, lengths in hydrogen Bohr radii, and magnetic fields in terms of the dimensionless quantity $\gamma = e\hbar B/2m_0cR_0$. The GaAs conduction-band effective-mass and dielectric constant are taken as $m_e = 0.0665$ (in units of the free electron mass m_0) and $\varepsilon = 12.5$, respectively, the relevant mass parameters are

$$1/m_{h\perp}^{\pm 3/2} = \gamma_1 - 2\gamma_2 \qquad 1/m_{h\parallel}^{\pm 3/2} = \gamma_1 + \gamma_2 \tag{2.8a}$$

$$1/m_{h\perp}^{\pm 1/2} = \gamma_1 + 2\gamma_2 \qquad 1/m_{h\parallel}^{\pm 1/2} = \gamma_1 - \gamma_2 \tag{2.8b}$$

the Luttinger valence-band parameters are taken from Bauer and Ando [13]: $\gamma_1 = 6.790$, $\gamma_2 = 1.924, \kappa = 1.2, q = 0.04$, and the g factor of the conduction-band electron is $g_e = -0.44$. In what follows, magnetoexciton energy states are labeled as $n\ell m(J_z^e, J_z^h)$ which correspond to an $n\ell m$-like exciton state composed of a J_z^e electron (with $J_z^e = \pm 1/2$) and a J_z^h hole (with $J_z^h = \pm 1/2, \pm 3/2$).

3. Results and discussion

We first compare our theoretical calculations for hh and lh $1s \rightarrow 2p_\pm$ and $1s \rightarrow 3p_\pm$ magnetoexciton transitions in a 125 Å GaAs–$Ga_{0.7}Al_{0.3}As$ QW under growth-direction applied

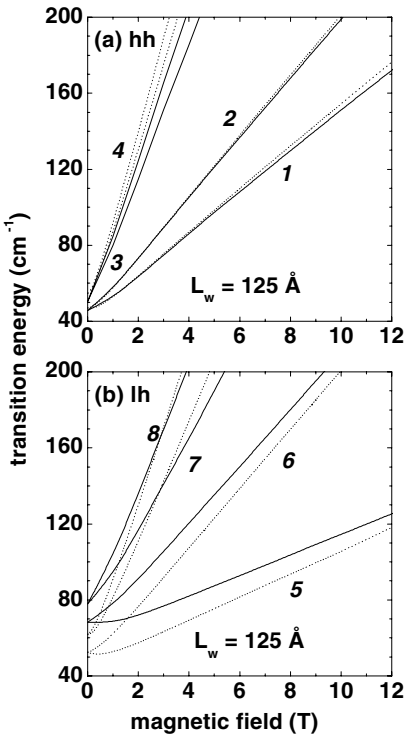

Figure 1. Heavy-hole (a) and light-hole (b) $1s\rightarrow 2p_{\pm}$ and $1s\rightarrow 3p_{\pm}$ calculated magnetoexciton spin-conserving transitions in a $L_w = 125$ Å (well width) GaAs–$Ga_{0.7}Al_{0.3}As$ QW, with the magnetic field applied along the growth direction of the heterostructure. Full curves are results of the present work with GaAs, AlAs and Luttinger parameters taken as in Duque *et al* [15] (shown as dotted curves). A magnetoexciton state is labeled as $n\ell m(J_z^e, J_z^h)$: a $n\ell m$-like exciton state with a J_z^e electron (with $J_z^e = \pm 1/2$) and a J_z^h hole (with $J_z^h = \pm 1/2, \pm 3/2$). Magnetoexciton heavy-hole transitions are 1: $1s\rightarrow 2p_-$ ($\pm 1/2, \pm 3/2$); 2: $1s\rightarrow 2p_+$ ($\pm 1/2, \pm 3/2$); 3: $1s\rightarrow 3p_-$ ($\pm 1/2, \pm 3/2$); 4: $1s\rightarrow 3p_+$ ($\pm 1/2, \pm 3/2$), and light-hole transitions are 5: $1s\rightarrow 2p_-$ ($\pm 1/2, \pm 1/2$); 6: $1s\rightarrow 2p_+$ ($\pm 1/2, \pm 1/2$); 7: $1s\rightarrow 3p_-$ ($\pm 1/2, \pm 1/2$); 8: $1s\rightarrow 3p_+$ ($\pm 1/2, \pm 1/2$).

magnetic field with the results recently obtained by Duque *et al* [15] (see figure 1). One should point out that, in the calculation by Duque *et al* [15], the exciton-envelope wavefunction is described as a product of variational hydrogenic-like wavefunctions and electron and hole *ground-state* solutions of the effective-mass equation for motion along the z-axis of the QW. In the present approach, the exciton wavefunction is written in terms of products of Gaussian functions with appropriate (cf equation (2.3)) hole and electron single-particle states (contribution of the *ground state and excited states*, cf equation (2.4)). For allowed spin-conserving transitions involving the lowest-energy exciton states, i.e. for the hh $1s \rightarrow 2p_{\pm}$ magnetoexciton transitions one finds very good agreement between the two calculations, whereas for higher-energy hh $1s \rightarrow 3p_{\pm}$ and lh $1s \rightarrow 2p_{\pm}$ and $1s \rightarrow 3p_{\pm}$ magnetoexciton transitions both theoretical approaches provide quantitatively different results. Of course, the present scheme is more reliable from the quantitative point of view, and better describes higher-energy states as the exciton-envelope wavefunction in equation (2.4) includes the effects of excited electron and hole single-particle in its expansion.

Results for the calculated hh $\rightarrow 2p_+$ magnetoexciton transition energies in GaAs–$Ga_{1-x}Al_xAs$ QWs of different well widths are shown in figure 2 as functions of the growth-direction applied magnetic field, together with the corresponding FIR data. From now on,

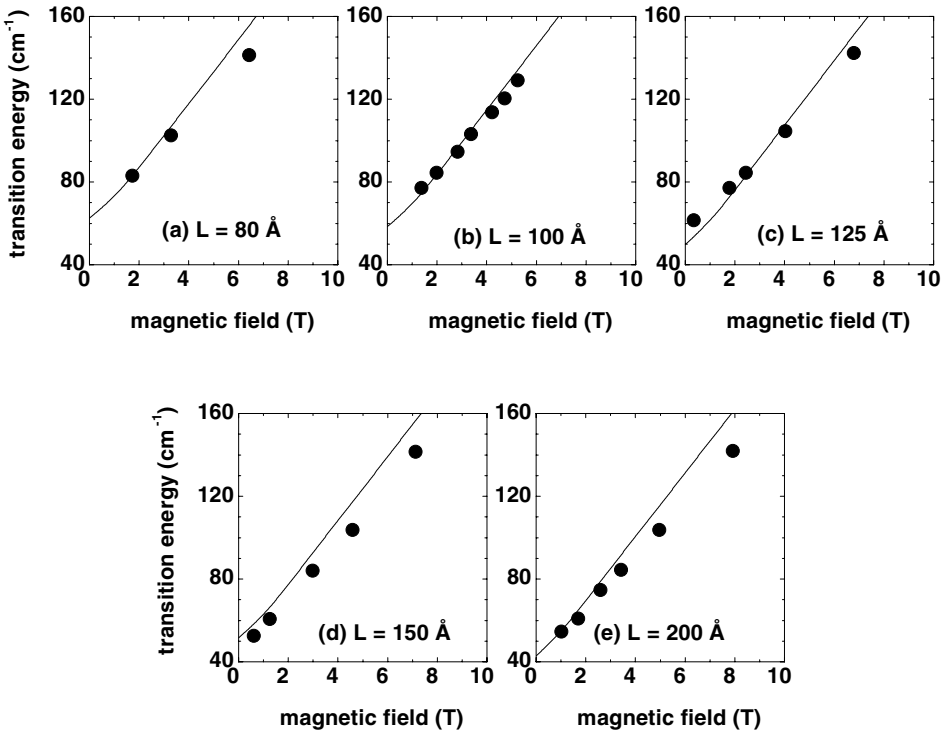

Figure 2. (a)–(c) Heavy-hole (full curves) spin-conserving $1s \rightarrow 2p_+$ theoretical magnetoexciton transition energies for GaAs–$Ga_{0.70}Al_{0.30}As$ QWs of different well widths as functions of the growth-direction applied magnetic field, together with experimental measurements by Cerne *et al* [8] and Nickel *et al* [4–6]; same $1s \rightarrow 2p_+$ transition energies for (d) $L = 150$ Å and (e) $L = 200$ Å GaAs–$Ga_{0.85}Al_{0.15}As$ QWs, with experimental data from Nickel *et al* [7].

unless otherwise stated, calculations are performed with GaAs, AlAs and Luttinger valence-band parameters taken as in Bauer and Ando [13]. Figure 2 indicates that agreement with experiment is fairly good, if one notes that actual FIR measurements are performed in GaAs–$Ga_{1-x}Al_xAs$ *multiple* QW samples, with $Ga_{1-x}Al_xAs$ barriers for which electron and hole tunneling effects are not to be disregarded (for example, the multiple QW sample [7] with well width $L_w = 150$ Å in figure 2(d) has a $Ga_{0.85}Al_{0.15}As$ barrier width of 100 Å), and that the present approach is only valid for *isolated* QWs.

The energies corresponding to lh and hh $1s \rightarrow 2p_\pm$ and $1s \rightarrow 3p_\pm$ magnetoexciton transitions are shown in figure 3(a) for a 80 Å GaAs–$Ga_{0.70}Al_{0.30}As$ QW. Notice that the experimental FIR data by Salib *et al* [4] are in fair agreement with intraexcitonic theoretical transitions, although any assignment of the experimental higher energy FIR data to specific magnetoexciton transitions is difficult to make. Also, the lh and hh $1s \rightarrow 2p_\pm$ magnetoexciton transition energies for a 100 Å GaAs–$Ga_{0.70}Al_{0.30}As$ QW (see figure 3(b)) are in quantitative agreement with FIR data by Cerne *et al* [8]. In particular, the higher-energy experimental transitions in figure 3(b), which Cerne *et al* [8] do not assign to any specific intraexcitonic transition, seem to correspond to lh $1s \rightarrow 2p_+$ theoretical magnetoexciton transitions, as may be concluded from an evaluation of the $\alpha(\omega)$ magneto-absorption coefficient for the intraexcitonic $1s \rightarrow np_\pm$ transitions. In the dipole approximation, $\alpha(\omega)$ is essentially given by

$$\alpha(\omega) \propto \frac{1}{\omega}\sum_f \left|\left\langle F^f_{J^e_z,J^h_z}(\vec{\rho},z_e,z_h)\middle|\hat{\varepsilon}\cdot\vec{\boldsymbol{P}}_r\middle|F^{1s}_{J^e_z,J^h_z}(\vec{\rho},z_e,z_h)\right\rangle\right|^2\delta(E_f - E_{1s} - \hbar\omega) \tag{3.1}$$

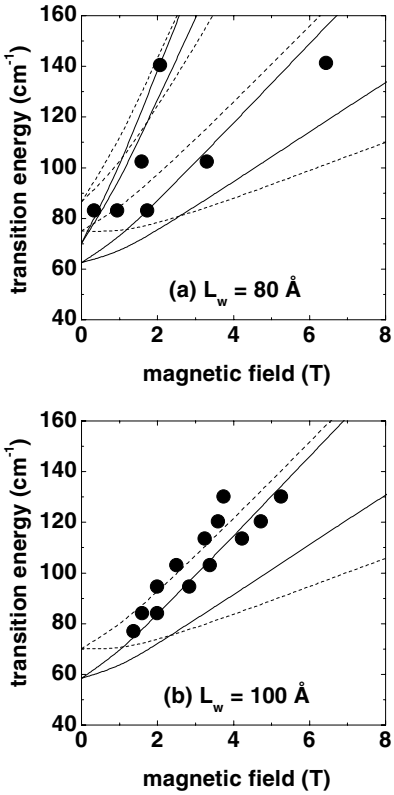

Figure 3. Light-hole (dashed curves) and heavy-hole (full curves) 1s $\rightarrow$ 2p$_\pm$ calculated magnetoexciton transition energies in (a) $L_w = 80$ Å and (b) $L_w = 100$ Å GaAs–$Ga_{0.7}Al_{0.3}As$ QWs; the magnetic field is applied along the growth direction of the heterostructure. In (a) we also show the 1s $\rightarrow$ 3p$_\pm$ calculated magnetoexciton transition energies. Experimental data are taken from Salib *et al* [4] and Cerne *et al* [8].

where $\hat{\varepsilon}$ corresponds to the photon polarization and $\vec{P}_r$ to the relative mechanical momentum of the e–h pair. Figure 4 displays the calculated lh and hh intraexcitonic magneto-absorption coefficient, for the case of left- and right-circularly polarized light in the well plane for a $L_w = 100$ Å GaAs–$Ga_{0.7}Al_{0.3}As$ QW. It is then clear that the oscillator strength of the lh and hh 1s $\rightarrow$ np$_\pm$ intraexcitonic transitions are of the same order of magnitude and that the lh 1s $\rightarrow$ 2p$_\pm$ transitions should therefore be experimentally observable. The calculated results in figure 4 unambiguously indicate that, if one performs the experiment with circularly polarized photons, both the lh and hh 1s $\rightarrow$ 2p$_-$ exciton transitions should be noticeable in the measured spectra. Also, one clearly sees (for $B = 1$, 2, and 3 T in figure 4) that weaker, higher energy features in $\alpha(\omega)$ corresponding to lh and hh 1s $\rightarrow$ 3p$_\pm$ transitions should be observable in the $L_w = 100$ Å sample, provided one is able to perform the experiment with higher spectral resolution; in fact, one notices that some of these higher energy transitions do show up in the experiment corresponding to the $L_w = 80$ Å sample (see figure 3(a)).

In figure 5(a), one notices that the 1s–2s energy separation obtained by Cerne *et al* [8] with PL and PLE measurements agrees well with the hh theoretical 1s–2s dispersion (separation of 60 cm^{-1} at zero magnetic field). Moreover, figure 5(b) unequivocally demonstrates that the lowest FIR frequency resonance measured by Cerne *et al* [8] is clearly due to free-electron CR and *not* to hh 2p$_-$ $\rightarrow$ 2s magnetoexciton transition energies, as suspected by Cerne *et al* [8].

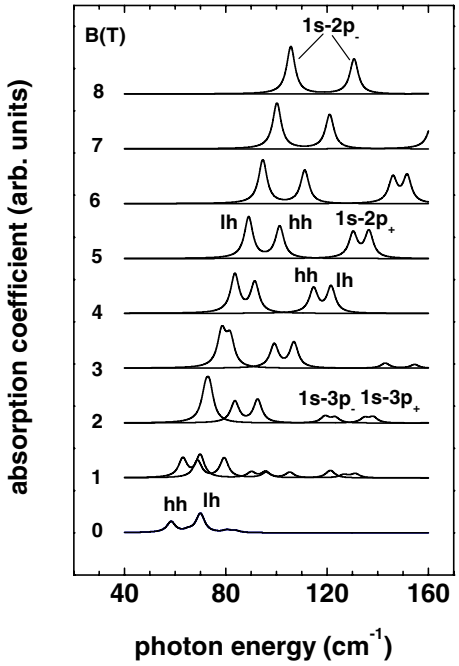

Figure 4. Intraexcitonic light-hole (lh) and heavy-hole (hh) 1s $\rightarrow$ $np_{\pm}$ magneto-absorption coefficient in a $L_w = 100$ Å GaAs–$Ga_{0.7}Al_{0.3}As$ QW, for the case of left- and right-circularly polarized light in the well plane; the magnetic field is applied along the growth direction of the heterostructure. The column of numbers on the left gives values of the applied magnetic field in Teslas (T).

The magnetic-field dependence of the magnetoexciton lh and hh 1s $\rightarrow$ $2p_{\pm}$ and 1s $\rightarrow$ $3p_{\pm}$ theoretical transition energies are shown in figure 6 for a $L_w = 125$ Å GaAs–$Ga_{0.70}Al_{0.30}As$ QW, and results are compared with the experimental FIR data by Nickel *et al* [4–7]. One notices that the FIR experimental data associated with the set of full squares are in adequate agreement with the 1s $\rightarrow$ $2p_+$ intraexcitonic hh theoretical transitions, as assigned by Nickel *et al* [4–7]. Also, solid experimental symbols appear to correspond to lh 1s $\rightarrow$ $2p_+$ and lh and hh 1s $\rightarrow$ $3p_{\pm}$ magnetoexciton transition energies, in contrast with the assignment to only hh transitions by Nickel *et al* [4–7]. However, the full up- and down-triangles of the FIR data by Nickel *et al* [4–7] are in clear disagreement with the theoretical magnetic-field dependence of the lh and hh 1s $\rightarrow$ $2p_-$ exciton transitions. We believe this discrepancy between the lower-energy theoretical transitions and FIR experiment is related to the fact that the present model calculation ignores hole–subband mixing, and certainly heavy and light holes should be strongly mixed when one deals with wide wells such as the present $L_w = 125$ Å QW. In order to mimic the above-mentioned hole mixing, one may choose to continue to work with the parabolic one-particle Hamiltonian and adequately change the effective-mass parameters (and the ε(GaAs) dielectric constant) in order to fit the FIR experimental (full symbols in figure 6) 1s $\rightarrow$ $2p_{\pm}$ transitions. Corresponding calculated results are shown in figure 7 for the $L_w = 125$ Å sample and in figure 8 for the $L_w = 150$ and 200 Å cases, with ε(GaAs) chosen as 12.7, 13.9, and 13.5, respectively, and the conduction-electron effective mass chosen as $0.073\,m_0$, $0.075\,m_0$ and $0.075\,m_0$, respectively. One should notice that the full down-triangles magnetic-field dependent experimental FIR energies correspond to 1s $\rightarrow$ $2p_-$ calculated

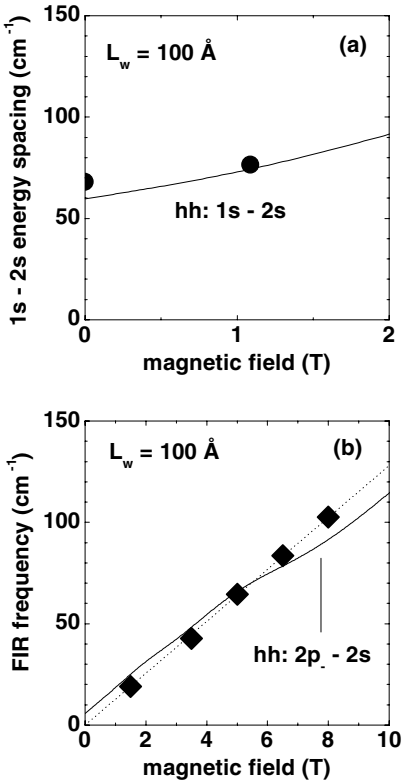

Figure 5. Results for a $L_{\rm w} = 100$ Å GaAs–$Ga_{0.7}Al_{0.3}As$ QW: (a) heavy-hole (full curve) $1s \rightarrow 2s$ calculated energy separation and experimental data (solid dots) deduced from interband PL excitation measurements by Cerne *et al* [8]; (b) heavy-hole (full curve) $2p_- \rightarrow 2s$ calculated magnetoexciton transition energies and free-electron CR with an effective mass of 0.073 m_0 (dotted curve), together with FIR resonance data (solid diamonds) by Cerne *et al* [8].

magnetoexciton transitions for valence-band effective masses of 0.3 m_0 for all three samples, i.e. for $L_{\rm w} = 125$, 150 and 200 Å, whereas the full up-triangles FIR data correspond to the $1s \rightarrow 2p_-$ transitions for valence-band effective masses chosen as 0.50 m_0, 0.79*s* m_0 and 0.45 m_0, respectively. The value of 0.79 m_0 for the valence-band in the case of $L_{\rm w} = 150$ Å is certainly peculiar, but it reflects the unexpected experimental behavior, i.e. in the case of the $L_{\rm w} = 150$ Å sample the difference of the $1s \rightarrow 2p_-$ experimental magnetoexciton transitions (up- and down-triangles) is higher than in the $L_{\rm w} = 200$ Å case in which the mixing of hh and lh should be stronger. Further studies are certainly necessary to clarify this point.

4. Summary and conclusions

Summing up, we have performed a theoretical study of confined magnetoexciton states in GaAs–$Ga_{1-x}Al_xAs$ QWs under magnetic fields applied perpendicular to the QW layers. We have worked in the effective-mass approximation and described the various exciton-envelope wavefunctions as products of electron and hole solutions of the associated quantum-well potentials and symmetry-adapted Gaussian functions. Magnetoexciton

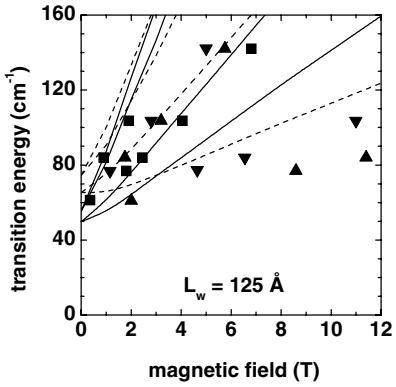

Figure 6. Light-hole (dashed curves) and heavy-hole (full curves) $1s \rightarrow 2p_{\pm}$ and $1s \rightarrow 3p_{\pm}$ calculated magnetoexciton transition energies in a $L_w = 125$ Å GaAs–$Ga_{0.7}Al_{0.3}As$ QW; the magnetic field is applied along the growth direction of the heterostructure. Also shown, the experimental measurements by Nickel *et al* [4–7].

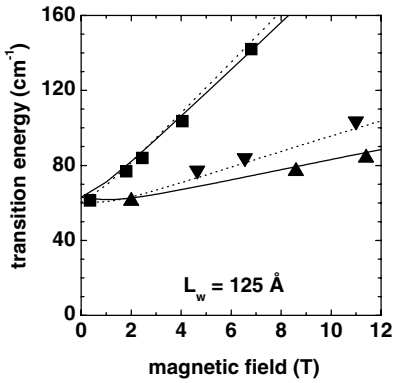

Figure 7. Heavy-hole $1s \rightarrow 2p_{\pm}$ magnetoexciton transition energies in a 125 Å well-width GaAs–$Ga_{0.7}Al_{0.3}As$ QW, with the magnetic field applied along the growth direction of the heterostructure, and calculated by assuming the in-plane heavy-hole mass as $0.50\,m_0$ (full curve) and $0.30\,m_0$ (dotted curve). Experimental data (solid symbols) are from Nickel *et al* [4–7].

envelope wavefunctions and energies are obtained by diagonalizing the appropriate exciton Hamiltonian. Exciton internal transitions are theoretically investigated by studying the allowed magnetoexcitonic transitions using far-infrared (terahertz) radiation circularly polarized in the plane of the QW. Theoretical results are obtained for intramagnetoexciton transition energies corresponding to excitations from 1s- like to 2s-, $2p_{\pm}$-, and $3p_{\pm}$-like magnetoexciton states, and from $2p_{-}$- to 2s-like states. We have also presented results for the $\alpha(\omega)$ magneto-absorption coefficient corresponding to the intraexcitonic $1s \rightarrow np_{\pm}$ transitions, in the dipole approximation, for the case of left- and right-circularly polarized photons. Finally, we have compared the present theoretical results with available optically detected resonance measurements, and obtained good overall agreement. Nevertheless, there are still several aspects of the magnetoexciton problem that are unclear or unexpected, and quite certainly, further experimental and theoretical studies are needed. In that sense, it would be of interest to perform experimental studies with right-, left- and linearly-polarized light in the plane of the QW, and investigate the possible observation of FIR features which could be unambiguously associated to lh CRs and lh intraexcitonic transitions.

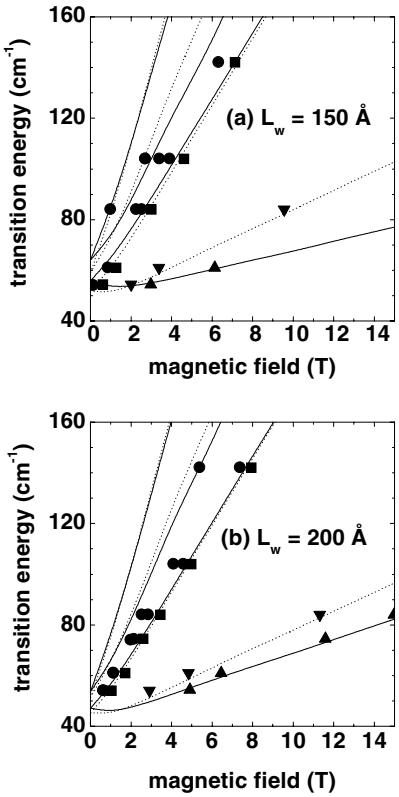

Figure 8. Heavy-hole $1s \rightarrow 2p_{\pm}$ and $1s \rightarrow 3p_{\pm}$ calculated magnetoexciton transition energies in (a) 150 Å and (b) 200 Å well-width GaAs–$Ga_{0.85}Al_{0.15}As$ QWs with the magnetic field applied along the growth direction of the heterostructure, and calculated by assuming the in-plane heavy-hole mass as (a) 0.79 m_0 (full curve) and 0.30 m_0 (dotted curve), and (b) 0.45 m_0 (full curve) and 0.30 m_0 (dotted line). Experimental data (solid dots) are from Nickel *et al* [7].

Acknowledgments

This research was supported in part by Red IX.E (CYTED), Millennium Scientific Iniciative (Condensed Matter Physics, grant P 99-135-F), Fondo Nacional de Ciencias (grant 1990271), and by the Universidad Santa Maria (internal grant). We are also grateful to Colombian (CODI-Universidad de Antioquia) and Brazilian Agencies (Fapesp, CNPq, and FAEP-UNICAMP) for partial financial support. CAD and LEO would like to thank the local hospitality of the Universidad Técnica Federico Santa María (Valparaíso, Chile), and Universidad de Santiago de Chile where part of this work was performed.

References

[1] Bastard G 1988 *Mechanics Applied to Semiconductor Heterostructures* (Les Ulis: Les Editions de Physique)
[2] Kelly M J 1995 *Low-Dimensional Semiconductors: Materials, Physics Technology, Devices* (Oxford: Clarendon)
[3] Hodge C C, Phillips C C, Skolnick M S, Smith G W, Whitehouse C R, Dawson P and Foxton C T 1990 *Phys. Rev.* B **41** 12 319

[4] Salib M S, Nickel H A, Herold G S, Petrou A, McCombe B D, Chen R, Bajaj K K and Schaff W 1996 *Phys. Rev. Lett.* **77** 1135
[5] Nickel H A, Herold G S, Salib M S, Kioseoglou G, Petrou A, McCombe B D and Broido D 1998 *Physica* B **249–51** 598
[6] Nickel H A, Herold G S, Yeo T, Kioseoglou G, Jiang Z X, McCombe B D, Petrou A, Broido D and Schaff W 1998 *Phys. Status Solidi* b **210** 341
[7] Nickel H A, Kioseoglou G, Yeo T, Cheong H D, Petrou A, McCombe B D, Broido D, Bajaj K K and Lewis R A 2000 *Phys. Rev.* B **62** 2773
[8] Cerne J, Kono J, Sherwin M S, Sundaram M, Gossard A C and Bauer G E W 1996 *Phys. Rev. Lett.* **77** 1131
[9] Kono J, Su M Y, Inoshita T, Noda T, Sherwin M S, Allen S J Jr and Sakaki H 1997 *Phys. Rev. Lett.* **79** 1758
[10] Kono J, Su M Y, Cerne J, Sherwin M S, Allen S J Jr, Inoshita T, Noda T and Sakaki H 1998 *Physica* B **249–51** 527
[11] Inoshita T and Sakaki H 1998 *Physica* B **249–51** 534
[12] Greene R L, Bajaj K K and Phelps D E 1984 *Phys. Rev.* B **29** 1807
Greene R L and Bajaj K K 1985 *Phys. Rev.* B **31** 6498
[13] Bauer G E W and Ando T 1988 *Phys. Rev.* B **38** 6015
[14] Andreani L C and Pasquarello S 1990 *Phys. Rev.* B **42** 8928
[15] Duque C A, Beltrán C L, Montes A, Porras-Montenegro N and Oliveira L E 2000 *Phys. Rev.* B **61** 9936
[16] Luttinger J M 1956 *Phys. Rev.* **102** 1030
[17] Bastard G, Mendez E E, Chang L L and Esaki L 1982 *Phys. Rev.* B **26** 1974
[18] Brown J W and Spector H N 1987 *Phys. Rev.* B **35** 3009
[19] Pacheco M, Barticevic Z and Claro F 1993 *J. Phys.: Condens. Matter* **5** A393
Barticevic Z, Pacheco M and Claro F 1995 *Phys. Rev.* B **51** 14 414
Pacheco M and Barticevic Z 1999 *J. Phys.: Condens. Matter* **11** 1079